

# Resolution and convergence requirements for extended overlap region in wall-bounded turbulence

Sergio Hoyas\*

*Instituto Universitario de Matemática Pura y Aplicada,  
Universitat Politècnica de València, Valencia 46022, Spain*

Ricardo Vinuesa†

*FLOW, Engineering Mechanics, KTH Royal Institute of Technology, SE-100 44, Stockholm, Sweden*

Victor Baxerres and Hassan Nagib‡

*Illinois Institute of Technology, Chicago, IL 60616*

(Dated: November 10, 2023)

Direct Numerical Simulations (DNSs) are one of the most powerful tools for studying turbulent flows. Even if the Reynolds numbers achievable with DNS are lower than those obtained with experimental means, there is a clear advantage since the entire velocity field is known, and any desired quantity can be evaluated. This also includes computation of derivatives of all relevant terms. One such derivative provides the indicator function, which may depend on mesh spacing and distribution, and the convergence of computation. The indicator function is a cornerstone to understanding inner and outer interactions in wall-bounded flows, and the description of the overlap region between them. We find dependence of the indicator function on the mesh distributions we examined, raising questions about the classical mesh and convergence requirements for DNS.

Since the early work by Kim, Moin, and Moser [1], direct numerical simulation (DNS) has become a widely used approach to study fundamental aspects of wall-bounded turbulence [2–7]. One topic within the study of wall-bounded turbulence that has received extensive attention from the research community due to its significant implications on flow representation and modeling is the overlap region of the mean velocity profile. In this overlap region, the large structures that populate the outer layer co-exist with the smaller ones strongly influenced by the wall and viscous effects. According to the classical literature, the mean velocity profile in this overlap region follows the well-known logarithmic law, which contains the von Kármán coefficient,  $\kappa$  [8, 9]:

$$\overline{U}_{x_{\text{in}}}^+(y^+ \gg 1) = \frac{1}{\kappa} \ln y^+ + B_0. \quad (1)$$

In this equation,  $\overline{U}_x$  is the streamwise mean velocity. The “in” subindex indicates that we are using the wall characterization of this velocity. The independent variable  $y^+$  is the inner-scaled wall-normal coordinate,  $y^+ = yu_\tau/\nu$ , where  $u_\tau$  is the friction velocity and  $\nu$  is the fluid kinematic viscosity.

Over the years, this has been a topic of active study, and universality of the log law and the von Kármán coefficient have been occasionally challenged or reaffirmed; e.g., see references [10–16]. Recently, Monkewitz and Nagib [17] (MN from now on) shed additional light on this topic, challenging the accumulated knowledge during the last century. MN’s main point is to consider in the inner asymptotic expansion a term proportional to the wall-normal coordinate,  $\mathcal{O}(Re_\tau^{-1})$ . Here  $Re_\tau = u_\tau \delta/\nu$  is the friction Reynolds number with  $\delta$  a characteristic outer length. This  $\delta$  can be thought of as the radius  $R$  in pipes, the semi-height in channels,  $h$ , or a length scale related to  $\delta_{99}$ . Following MN, the pure log law is not observed in channels and pipes (as well as other flows with streamwise pressure gradients) if  $Re_\tau$  is not above  $\mathcal{O}(10^4)$ . MN’s extended matched asymptotics reveals an additional term in the expansion of the velocity for this layer leading to an extra contribution in the overlap layer in the form  $S_0 y^+ Re_\tau^{-1}$ , where  $S_0$  is a coefficient.

Interestingly, the overlap region represented by a combined logarithmic and linear terms exhibits values of the von Kármán coefficient  $\kappa$  consistent with those obtained from skin-friction relations, a fact that suggests that this approach can reveal high- $Re$  trends even at moderate Reynolds numbers. The main point of this matched asymptotics theory is to use a new expression in the overlap region for  $\overline{U}_x$ . MN’s formula reads:

$$\overline{U}_{x_{\text{in}}}^+(y^+ \gg 1) \sim \kappa^{-1} \ln y^+ + B_0 + B_1/Re_\tau + S_0 y^+/Re_\tau. \quad (2)$$

To obtain accurate values of these coefficients, it is necessary to address two fundamental issues:

---

\* serhocal@mot.upv.es

† rvinuesa@mech.kth.se

‡ nagib@iit.edu

Case	$Re_\tau$	$L_x/\delta$	$L_z/\delta$	$\Delta x^+$	$\Delta(R\theta^+)$	$\max(\Delta y^+)$	$\min(\Delta y^+)$	$N_x$	$N_z$	$N_y$	ETT	$\epsilon$
PLRF	549	$10\pi$	$2\pi$	5.62	3	3.2	0.018	3072	1152	256	93	$1.2 \times 10^{-4}$
PHRF	549	$10\pi$	$2\pi$	5.62	3	1.6	0.005	3072	1152	512	87	$2.6 \times 10^{-4}$
PLRC	549	$10\pi$	$2\pi$	11.2	4.5	3.2	0.018	1536	768	256	184	$8.2 \times 10^{-5}$
PHRC	549	$10\pi$	$2\pi$	11.2	4.5	1.6	0.005	1536	768	512	56	$3.8 \times 10^{-4}$
CLRC	546	$8\pi$	$3\pi$	9	5	5.85	0.8	1536	1152	251	150	$7.6 \times 10^{-5}$
CHRC	546	$8\pi$	$3\pi$	9	5	1.68	0.05	1536	1152	901	150	$3.8 \times 10^{-5}$

TABLE I: Summary of the simulations discussed in this work, where ‘P’ stands for pipe and ‘C’ for channel. The nomenclature ‘LR’ and ‘HR’ stands for low and high resolution in  $y$ , whereas ‘C’ and ‘F’ denote coarse and fine in  $x$  and  $z$ . Note that  $L_x$  and  $L_z$  are the periodic streamwise and spanwise dimensions while  $h$  is the channel half height.  $\Delta x^+$  and  $\Delta z^+$  are the inner-scaled resolutions in terms of dealiased Fourier modes. The wall-normal direction is indicated in both flows by  $y$ .  $N_x, N_z$ , and  $N_y$  are the numbers of collocation points in the three different directions. The time span of the simulation is given in terms of eddy turnovers  $u_\tau T/\delta$ , and  $\epsilon$  is a measure of convergence, defined in [18]. Colors given in the first column are used throughout the paper, using dashed lines for the channel.

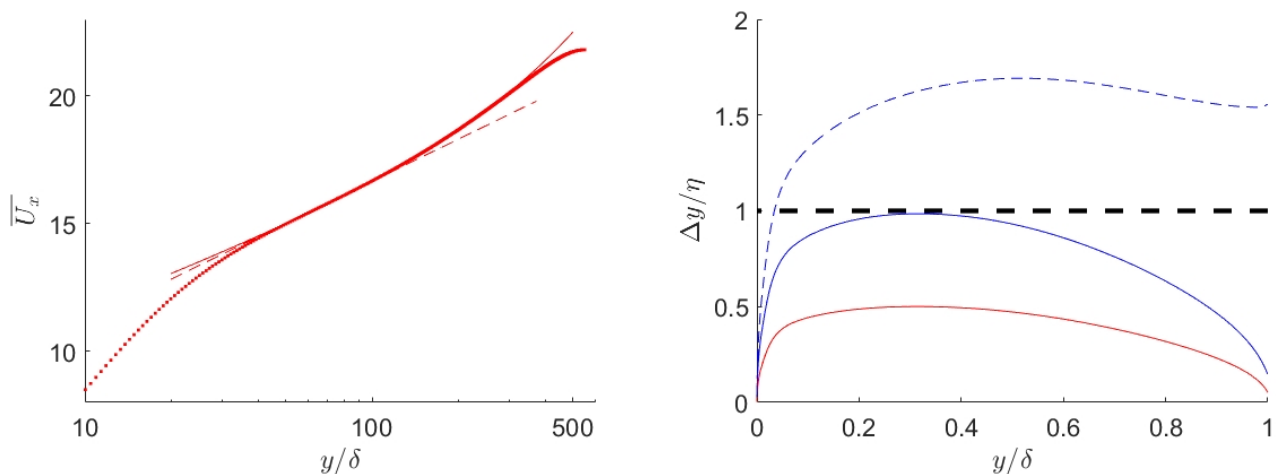


FIG. 1: (Left) Streamwise velocity for the PHRF case (thick line), together with the pure log (dashed line) and log-plus-linear (thin line) overlap layers. (Right) Grid distance in the wall-normal direction, scaled with the Kolmogorov length. Colors as in Table 1, where solid denotes pipe and dashed channel.

1. To find  $\kappa$ , the challenge is to identify the location and extent of the overlap region, which is weakly dependent on the Reynolds number [17].
2. To obtain the correct value of  $S_0$ , it is necessary to obtain with high accuracy the values of  $d\overline{U}_x^+/dy^+$ .

Focusing on the second point above, it is possible to obtain an equation for the value of  $\kappa$  and  $S_0$  through the indicator function:

$$\Xi(y^+) = y^+ \frac{d\overline{U}_x^+}{dy^+}. \quad (3)$$

From equations (2) and (3), one can obtain the equation for  $\kappa$  and  $S_0$ :

$$\Xi(y^+) = \kappa^{-1} + S_0 y^+ / Re_\tau.$$

Thus, to accurately determine  $S_0$ , it is necessary to compute the indicator function with high accuracy, an aspect which has not been sufficiently investigated in the literature. While a convergence criterion exists for fully developed flows [18], and the domain size of the problem has been examined in depth [19, 20], the necessary grid spacing has received much less attention. Examples can be found in some very large simulations [7, 21], where the authors only report their mesh size and compare their results with those in previous references, which basically do the same.

We have performed two different numerical experiments to examine this issue and its implications. The details can be found in Table 1. On the one hand, we have studied a smooth pipe of radius  $R$  and length  $L_x = 10\pi R$  for

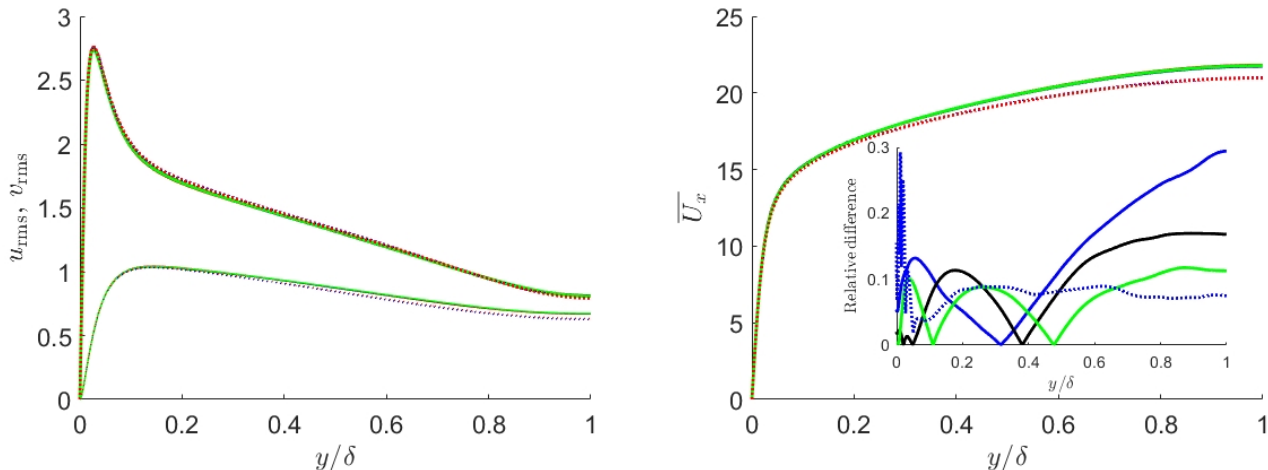


FIG. 2: (Left) Intensities in the wall-normal and streamwise directions for all cases. (Right)  $\overline{U}_x$ . The box shows the difference between the finer case and the others. Colors as in Table 1. Continuous lines, pipes. Dotted lines, channels

$Re_\tau = 550$ . We will use  $y$  to indicate the distance to the wall. We have used four different meshes, as seen in Table 1. The base mesh is the case PLRC with the same resolution in  $x$  and  $R\Theta$  as a channel. On the other hand, the mesh in the radial direction has twice the number of points needed in a channel due to the skewness of the cells near the pipe center. The details of the mesh can be seen in right side of Figure 1. Note that for the pipe cases, the wall-normal grid spacing is below the Kolmogorov scale throughout the computational domain. Starting with the PLRC, we doubled the cells in the radial direction (PHRC), azimuthal, and streamwise directions (PLRF), and all of them (PHRF). All these simulations ran for at least 55 eddy-turnover times (ETT), defined as  $ETT = Tu_\tau/R$ .

On the other hand, we have run two channel-flow simulations. The first one (CLRC) is a simulation with the same mesh as Jiménez and Hoyas [22, 23]. The second one (CHRC) uses a mesh considered enough for  $Re_\tau = 3000$  [19, 24]. Two different codes were employed. OpenpipeFlow was used to run the pipe simulations [21, 25]. The code LISO was used for running the channel flow [2, 26, 27]. Both codes employ Fourier-decomposition techniques in the streamwise and spanwise directions. Openpipeflow uses a seventh-order finite-difference scheme in the wall-normal direction, while LISO uses a tenth-order compact-finite-difference scheme [26, 28].

In the case of the pipe flow, the difference among the four simulations appears small when analyzing the streamwise and wall-normal fluctuations, as displayed in Figure 2 (left), and the streamwise velocity, Figure 2 (right). As shown in the latter, the difference between the coarser cases and the finer ones is below 0.3% everywhere. Such accuracy, however, is not sufficient for utilizing the indicator function  $\Xi$  to extract reliable coefficients of overlap region. As shown in Figure 3 (left), the different curves of  $\Xi$  do not collapse exactly in the region between  $y/\delta = 0.3$  and  $y/\delta = 0.5$ , where the slope value of  $\Xi$  is critical. This is more clearly appreciated in Figure 3 (right), where the differences across cases can be more clearly assessed. Notice that the finer mesh, PHRF case, corresponds to the solid red line. The other three cases have not converged to the PHRF's value even after 100 ETT. A better agreement is found in the case of the channels. Here, the convergence at  $y/h = 0.35$  is obtained after approximately 15 ETT. However, at  $y/h = 0.45$  the differences are of the order of 2% after 80 ETT, which is an extremely lengthy computation for high-Reynolds-number simulations.

The effect of this lack of adequate resolution can be better evaluated by the time-averaged values of the overlap coefficients  $\kappa$ ,  $B$ , and  $S_0$  as functions of ETT. After 50 ETTs, the differences among the cases are still above 3%, as shown in Figure 4. Again, the convergence for the channel case is better, but there remains a small difference up to ETT of 150, which corresponds to very expensive computations. In any case, at least 20 ETTs are needed to obtain some level of convergence. Such differences in the indicator function  $\Xi$  should be smaller for any reliable simulation to predict the values of  $\kappa$ ,  $B$ , and  $S_0$ .

Finally, in the case of pipe flow, the values of these coefficients appear to depend on the azimuthal resolution, raising questions about the mesh aspect ratio of the grids. A careful study of such mesh variation effects in flows near their singularities, as in case around the axis of pipes, is highly recommended. Such a study should also examine the sensitivity of the indicator function  $\Xi$  to the order of the finite difference scheme used in the DNS. In general, the results demonstrate that classical and commonly mesh size in the wall-normal direction for DNSs are not sufficiently fine to extract coefficients of the overlap region in wall-bounded turbulent flows, such as the the von Kármán coefficient,  $\kappa$ .

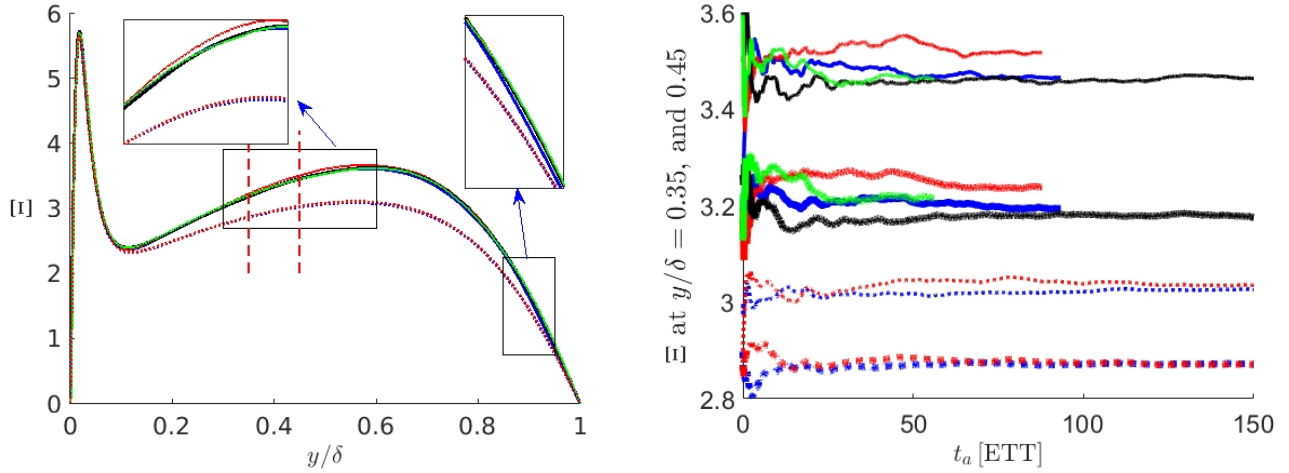


FIG. 3: (Left)  $\Xi$  for the six case under study. (Right) Values of  $\Xi$  at  $y/\delta = 0.35$  and  $0.45$  as a function of the averaging time  $t_a$  expressed in eddy-turnover times (ETT). Colors as in Table 1. Continuous lines, pipes. Dotted lines, channels. Thick lines,  $y/\delta = 0.35$ . Thin lines,  $y/\delta = 0.45$ .

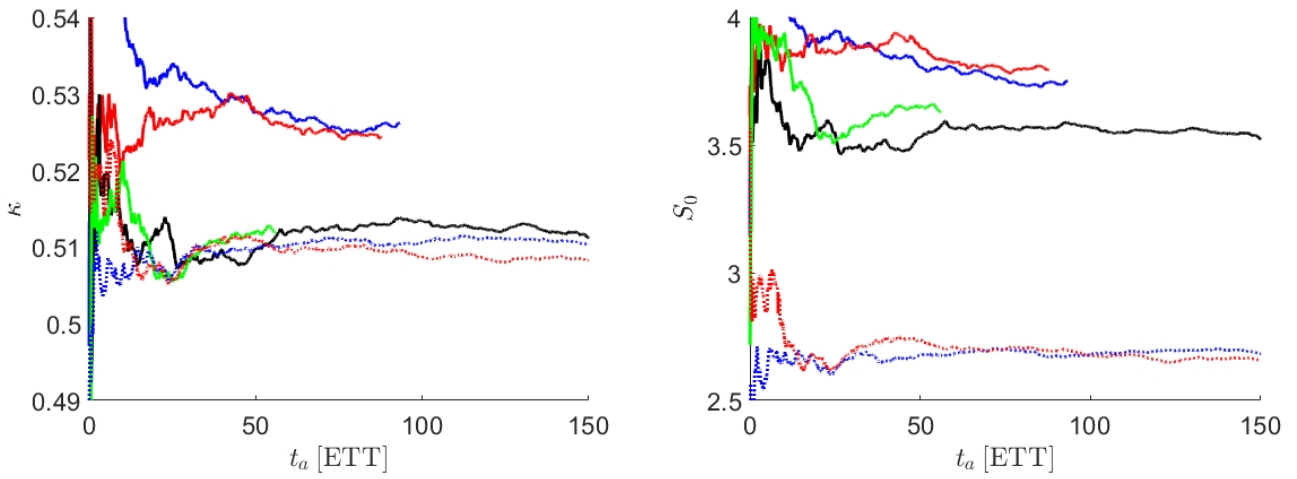


FIG. 4:  $\kappa$  (Left) and  $S_0$  (Right) for the six cases under study as functions of the averaging time  $t_a$  expressed in ETT. Colors as in Table 1. Continuous lines, pipes. Dotted lines, channel

In conclusion, DNSs still stand as a powerful tool for the exploration of turbulent flows. However, the accuracy of DNS to compute certain important derivatives such as those required for the indicator function  $\Xi$  is challenged. To calculate  $\Xi$ , accurate values of the wall-normal derivative of the streamwise velocity must be established. Our investigation reveals that the indicator function exhibits sensitivity around the classic mesh size commonly used in DNSs. In particular, several coefficients of the overlap region required for the Monkewitz and Nagib's model of wall-bounded flows under streamwise pressure gradients [17] cannot be found with less than 3% difference among the various meshes we tested. For example, this creates a new uncertainty source in the estimation of the von Kármán coefficient that is very important for modeling and predictiong wall-bounded turbulent flows. This uncertainty can be also generalized to any quantity needing wall-normal derivatives.

**Data availability:** The data used for this paper can be obtained by contacting S. Hoyas at serhocal@mot.upv.es.

## ACKNOWLEDGMENTS

For computer time, this research used the resources of the Supercomputing Laboratory at King Abdullah University of Science & Technology (KAUST) in Thuwal, Saudi Arabia, Project K1652. RV acknowledges the financial support from ERC grant no. ‘2021-CoG-101043998, DEEPCONTROL’. Views and opinions expressed are however those of the author(s) only and do not necessarily reflect those of European Union or European Research Council. Neither the European Union nor granting authority can be held responsible for them. SH is funded by project PID2021-128676OB-I00 by Ministerio de Ciencia, innovación y Universidades / FEDER.

- 
- [1] J. Kim, P. Moin, and R. Moser, Turbulence statistics in fully developed channels flows at low Reynolds numbers, *J. Fluid Mech.* **177**, 133 (1987).
  - [2] S. Hoyas and J. Jiménez, Scaling of the velocity fluctuations in turbulent channels up to  $Re_\tau = 2003$ , *Phys. Fluids* **18**, 011702 (2006).
  - [3] P. R. Spalart and J. H. Watmuff, Experimental and numerical study of a turbulent boundary layer with pressure gradients, *J. Fluid Mech.* **249**, 337 (1993).
  - [4] J. Sillero, J. Jiménez, and R. D. Moser, One-point statistics for turbulent wall-bounded flows at Reynolds numbers up to  $\delta^+ \approx 2000$ , *Phys. Fluids* **25**, 105102 (2013).
  - [5] S. Pirozzoli, J. Romero, M. Fatica, R. Verzicco, and P. Orlandi, One-point statistics for turbulent pipe flow up to  $re_\tau \approx 6000$ , *J. Fluid Mech.* **926**, A28 (2021).
  - [6] R. Vinuesa, S. M. Hosseini, A. Hanifi, D. S. Henningson, and P. Schlatter, Pressure-gradient turbulent boundary layers developing around a wing section, *Flow Turbul. Combust.* **99**, 613 (2017).
  - [7] S. Hoyas, M. Oberlack, F. Alcántara-Ávila, S. V. Kraheberger, and J. Laux, Wall turbulence at high friction Reynolds numbers, *Phys. Rev. Fluids* **7**, 014602 (2022).
  - [8] T. von Kármán, Turbulence and skin friction, *J. Aero. Sci.* **1**, 1 (1934).
  - [9] C. M. Millikan, A critical discussion of turbulent flows in channels and circular tubes, In *Proc. 5th Int. Congr. Appl. Mech.*, Wiley, NY (1938).
  - [10] W. K. George and L. Castillo, Recent advancements toward the understanding of turbulent boundary layers, *AIAA J.* **44**, 2435 (2006).
  - [11] G. I. Barenblatt, A. J. Chorin, and V. M. Prostokishin, A note on the intermediate region in turbulent boundary layers, *Phys. Fluids* **12**, 2159 (2000).
  - [12] P. A. Monkewitz, K. A. Chauhan, and H. M. Nagib, Comparison of mean flow similarity laws in zero pressure gradient turbulent boundary layers, *Phys. Fluids* **20**, 105102 (2008).
  - [13] R. Vinuesa, P. Schlatter, and H. M. Nagib, Role of data uncertainties in identifying the logarithmic region of turbulent boundary layers, *Exp. Fluids* **55**, 1751 (2014).
  - [14] H. M. Nagib and K. A. Chauhan, Variations of von Kármán coefficient in canonical flows, *Phys. Fluids* **20**, 101518 (2008).
  - [15] P. Luchini, Universality of the turbulent velocity profile, *Phys. Rev. Lett.* **118**, 224501 (2017).
  - [16] M. Oberlack, S. Hoyas, S. V. Kraheberger, F. Alcántara-Ávila, and J. Lawx, Turbulence statistics of arbitrary moments of wall-bounded shear flows: A symmetry approach, *Phys. Rev. Lett.* **128**, 024502 (2022).
  - [17] P. Monkewitz and H. Nagib, The hunt for the Kármán ‘constant’ revisited, *J. Fluid Mech.* **967**, A15 (2023).
  - [18] R. Vinuesa, C. Prus, P. Schlatter, and H. Nagib, Convergence of numerical simulations of turbulent wall-bounded flows and mean cross-flow structure of rectangular ducts, *Meccanica* **51**, 3025 (2016).
  - [19] A. Lozano-Durán and J. Jiménez, Effect of the computational domain on direct simulations of turbulent channels up to  $Re_\tau = 4200$ , *Phys. Fluids* **26**, 011702 (2014).
  - [20] F. Llesma-Rodríguez, S. Hoyas, and M. Pérez-Quiles, Influence of the computational domain on DNS of turbulent heat transfer up to  $Re_\tau = 2000$  for  $Pr = 0.71$ , *Int. J. Heat Mass Transf.* **122**, 983 (2018).
  - [21] J. Yao, S. Rezaeiravesh, P. Schlatter, and F. Hussain, Direct numerical simulations of turbulent pipe flow up to  $Re_\tau \approx 5200$ , *J. Fluid Mech.* **956**, A18 (2023).
  - [22] S. Hoyas and J. Jiménez, Reynolds number effects on the Reynolds-stress budgets in turbulent channels, *Phys. Fluids* **20**, 101511 (2008).
  - [23] J. Jiménez and S. Hoyas, Turbulent fluctuations above the buffer layer of wall-bounded flows, *J. Fluid Mech.* **611**, 215 (2008).
  - [24] F. Alcántara-Ávila, S. Hoyas, and M. Pérez-Quiles, Direct Numerical Simulation of thermal channel flow for  $Re_\tau = 5000$  and  $Pr = 0.71$ , *J. Fluid Mech.* **916**, A29 (2021).
  - [25] A. P. Willis, The Openpipeflow Navier–Stokes solver, *SoftwareX* **6**, 124 (2017).
  - [26] F. Llesma-Rodríguez, F. Alcántara Ávila, M. Pérez-Quiles, and S. Hoyas, A code for simulating heat transfer in turbulent channel flow, *Mathematics* **9**, 10.3390/math9070756 (2021).
  - [27] L. Yu, M. Z. Yousif, M. Zhang, S. Hoyas, R. Vinuesa, and H.-C. Lim, Three-dimensional esrgan for super-resolution reconstruction of turbulent flows with tricubic interpolation-based transfer learning, *Phys. Fluids* **34** (2022).
  - [28] S. K. Lele, Compact finite difference schemes with spectral-like resolution, *Journal of Computational Physics* **103**, 16

(1992).